







One-step ethylene production from a four-component gas mixture by a single physisorbent

Jian-Wei Cao ^{1,6}, Soumya Mukherjee ^{2,3,6}, Tony Pham ⁴, Yu Wang¹, Teng Wang¹, Tao Zhang ¹, Xue Jiang¹, Hui-Juan Tang¹, Katherine A. Forrest⁴, Brian Space^{4,5}, Michael J. Zawortko ²✉ & Kai-Jie Chen ¹✉

One-step adsorptive purification of ethylene (C₂H₄) from four-component gas mixtures comprising acetylene (C₂H₂), ethylene (C₂H₄), ethane (C₂H₆) and carbon dioxide (CO₂) is an unmet challenge in the area of commodity purification. Herein, we report that the ultramicroporous sorbent Zn-atz-oba (H₂oba = 4,4-dicarboxyl diphenyl ether; Hatz = 3-amino-1,2,4-triazole) enables selective adsorption of C₂H₂, C₂H₆ and CO₂ over C₂H₄ thanks to the binding sites that lie in its undulating pores. Molecular simulations provide insight into the binding sites in Zn-atz-oba that are responsible for coadsorption of C₂H₂, C₂H₆ and CO₂ over C₂H₄. Dynamic breakthrough experiments demonstrate that the selective binding exhibited by Zn-atz-oba can produce polymer-grade purity (>99.95%) C₂H₄ from binary (1:1 for C₂H₄/C₂H₆), ternary (1:1:1 for C₂H₂/C₂H₄/C₂H₆) and quaternary (1:1:1:1 for C₂H₂/C₂H₄/C₂H₆/CO₂) gas mixtures in a single step.

¹Key Laboratory of Special Functional and Smart Polymer Materials of Ministry of Industry and Information Technology, Xi'an Key Laboratory of Functional Organic Porous Materials, School of Chemistry and Chemical Engineering, Northwestern Polytechnical University, Xi'an, Shaanxi, PR China. ²Bernal Institute, Department of Chemical Sciences, University of Limerick, Limerick, Republic of Ireland. ³Department of Chemistry, Technical University of Munich, Garching b, München, Germany. ⁴Department of Chemistry, University of South Florida, Tampa, FL, USA. ⁵Department of Chemistry, North Carolina State University, Raleigh, USA. ⁶These authors contributed equally: Jian-Wei Cao, Soumya Mukherjee. ✉email: xtal@ul.ie; ckjiscon@nwpu.edu.cn

Ethylene (C_2H_4) is a feedstock for the production of plastics, detergents and coatings and its production, now approaching 200 million tons per year, continues to grow¹. The energy footprints for purification of C_2H_4 and propylene (C_3H_6), also one of the highest volume products of the chemical industry, account for *ca.* 0.3% of the global energy demand². The presence of impurities is a consequence of the steam pyrolysis process used to produce C_2H_4 , which in turn results in acetylene (C_2H_2), carbon dioxide (CO_2), ethane (C_2H_6) and other downstream products including propylene (C_3H_6), propane (C_3H_8), hydrogen (H_2), C4 and higher light hydrocarbons^{3,4}, which are easily separated by the difference of boiling points. Polymer-grade (>99.95% purity) C_2H_4 is generated by stepwise removal in downstream purification processes: CO_2 is removed using caustic soda; C_2H_2 is eliminated via catalytic hydrogenation with noble-metal catalysts at high temperature and pressure; cryogenic distillation is typically employed to remove C_2H_6 ⁵.

To mitigate the high energy footprint of C_2H_4 production, researchers have typically focused upon the development of a new generation of physisorbents that exhibit affinity for one gas over others in a gas mixture. The promise of physisorbents lies with their relatively low energy consumption compared to distillation processes thanks to facile regeneration/recycling⁶. However, physisorbents tend to be unsuitable for ethylene purification because the kinetic diameter of C_2H_4 (4.1 Å) sits between CO_2 (3.3 Å), C_2H_2 (3.3 Å) and C_2H_6 (4.4 Å), precluding the possibility of molecular sieving by pore size engineered physisorbents⁷. Since the quadrupole moment of C_2H_4 (1.5×10^{-26} esu cm²) also lies between CO_2 (4.3×10^{-26} esu cm²), C_2H_2 (7.2×10^{-26} esu cm²) and C_2H_6 (0.65×10^{-26} esu cm²)⁸, one-step purification of C_2H_4 by thermodynamics (selective binding) has thus far proven to be elusive. Metal organic materials (MOMs)⁹, also called metal-organic frameworks (MOFs)^{10,11} or porous coordination polymers (PCPs)¹², have promising applications as C_2 and CO_2 selective physisorbents for several binary mixtures, including C_2H_2/C_2H_4 , C_2H_4/C_2H_6 , C_2H_6/C_2H_4 , C_2H_2/CO_2 and CO_2/C_2H_2 ^{13–34}. There are also examples of physisorbents that are effective against ternary C_2 and C_2-CO_2 mixtures such as $C_2H_2/C_2H_4/C_2H_6$ and $C_2H_2/C_2H_4/CO_2$ ^{35–41}. Certain classes of physisorbents are amenable to systematic fine-tuning of pore chemistry and pore size^{42,43} and have resulted in “second generation” sorbents with > one order of magnitude improvement in performance^{18,24,44,45,47}. Nevertheless, we are aware of only one report of C_2H_4 purification from quaternary mixtures using physisorbents as reported by us in 2019 by introducing the synergistic sorbent separation technology (SSST)⁴⁶ concept, which enables one-step production of high-purity ethylene from a quaternary $C_2H_2-C_2H_4-C_2H_6-CO_2$ mixture by exploiting three benchmark sorbents, Zn-atz-*ipa*, SIFSIX-3-Ni, and TIFSIX-2-Cu-i. These sorbents were tandem-packed in a single column to sequentially remove C_2H_6 , CO_2 , and C_2H_2 , respectively (Fig. 1). Unfortunately, the interplay of packing sequence and gas mass transfer in SSST can make industrial-scale processes infeasible and, as illustrated in Fig. 1, a single sorbent that coadsorbs C_2H_2 , C_2H_6 , and CO_2 would be desirable for quaternary gas separations such as the purification of C_2H_4 from a $C_2H_2-C_2H_4-C_2H_6-CO_2$ mixture. Herein we report that the challenge of one-step C_2H_4 purification from a quaternary mixture ($C_2H_2-C_2H_4-C_2H_6-CO_2$) is achieved by a single physisorbent, the ultramicroporous coordination network Zn-atz-*oba*.

Results

Synthesis and characterization of Zn-atz-*oba*. Zn-atz-*oba* was synthesized following a previously reported protocol (for details see Methods section)⁴⁷. The bulk phase purity of crystalline

samples was confirmed by powder X-ray diffraction, PXRD (Fig. 2c). As shown in Fig. 2a, b, Zn(II) cations are linked by atz[−] anions to form 2D undulating layers with dinuclear Zn(II) clusters as nodes. These layers are further cross-linked via *oba*^{2−} ligands to form a pcu topology network. As revealed by thermogravimetric analysis (Supplementary Fig. 1), activated Zn-atz-*oba* is fully desolvated and stable until *ca.* 673 K. As calculated by PLATON⁴⁸, the void space of Zn-atz-*oba* is 35.9%.

The pore volume, Langmuir and Brunauer–Emmett–Teller (BET) specific surface area for Zn-atz-*oba* are $0.287 \text{ cm}^3 \text{ g}^{-1}$, $783.1 \text{ m}^2 \text{ g}^{-1}$, and $710.7 \text{ m}^2 \text{ g}^{-1}$, respectively, as calculated from its cryogenic (77 K) N_2 adsorption isotherm (Supplementary Figs. 2–4). Both parameters are in agreement with the crystal structure derived pore volume ($0.283 \text{ cm}^3 \text{ g}^{-1}$) and the Langmuir surface area calculated therefrom ($755 \text{ m}^2 \text{ g}^{-1}$), respectively. Horvath-Kawazoe model (pore geometry: slit) based pore size distribution analysis revealed the aperture distribution to be ultramicroporous between 0.32 and 0.44 nm (Supplementary Fig. 5).

Adsorption isotherm, selectivity, and enthalpy. The C_2H_2 , C_2H_4 , C_2H_6 , and CO_2 adsorption isotherms of activated Zn-atz-*oba* were recorded at 298 and 273 K (Fig. 2e and Supplementary Fig. 6). Interestingly, C_2H_2 , C_2H_6 , and CO_2 exhibited higher adsorption uptakes at 298 K across the entire pressure range tested, 0–100 kPa, especially in the low-pressure region, 0–20 kPa. These uptakes suggest selective adsorption of C_2H_2 , CO_2 , and C_2H_6 over C_2H_4 by Zn-atz-*oba*. Low-coverage isosteric adsorption enthalpies were determined by virial fit of the isotherm data (see Methods section, Supplementary Note 2: Adsorption enthalpy calculation, and Supplementary Figs. 7–10) and the trends (Fig. 2d) correlate well with their low-pressure (until 20 kPa) saturation uptake capacities as follows: $Q_{st}(C_2H_6)$ (30.0 kJ mol^{-1}) > $Q_{st}(CO_2)$ (29.0 kJ mol^{-1}) > $Q_{st}(C_2H_2)$ (27.5 kJ mol^{-1}) > $Q_{st}(C_2H_4)$ (27.0 kJ mol^{-1}). We also note that the adsorption enthalpies of all four gases are below 35 kJ mol^{-1} , an indication that Zn-atz-*oba* should exhibit a relatively low energy footprint for regeneration^{27,45}.

Adsorption selectivity is also a key indicator of separation performance. The adsorption selectivities of Zn-atz-*oba* for C_2H_2/C_2H_4 , C_2H_6/C_2H_4 , and CO_2/C_2H_4 were calculated using Ideal Adsorbed Solution Theory⁴⁹ (IAST) after fitting the single-component adsorption isotherms to the Langmuir-Freundlich model (Supplementary Figs. 11–14 and Supplementary Table 1). As shown in Fig. 2f, at 298 K and 100 kPa, the selectivities are 1.43 (C_2H_2/C_2H_4), 1.27 (C_2H_6/C_2H_4), and 1.33 (CO_2/C_2H_4). C_2H_6/C_2H_4 and C_2H_2/C_2H_4 selectivities for Zn-atz-*oba* are comparable to the current benchmark sorbents that enable C_2H_4 purification from $C_2H_2/C_2H_4/C_2H_6$ 1:1:1 ternary mixtures (1.2 and 1.8 for TJT-100³⁵, 1.46 and 1.09 for Azole-Th-1³⁶, 1.32 and 1.4 for NPU-1³⁹, 1.4 and 1.07 for UPC-612 and 1.5 and 1.4 for UPC-613⁴¹, respectively) (Supplementary Table 3). The selectivity for CO_2/C_2H_4 is also comparable to that of C_2H_6/C_2H_4 and C_2H_2/C_2H_4 . Grand canonical Monte Carlo (GCMC) simulations of binary mixtures containing 1:1 C_2H_2/C_2H_4 , C_2H_6/C_2H_4 , and CO_2/C_2H_4 in Zn-atz-*oba* confirmed that these selectivities are greater than 1 at 298 K and 1 atm (Supplementary Table 5). These selectivities and relatively close adsorption enthalpies suggest that Zn-atz-*oba* might coadsorb the preferred sorbates C_2H_2 , C_2H_6 , and CO_2 when subjected to a mixture feed.

Mechanism of gas adsorption by GCMC simulations. GCMC simulations were conducted upon Zn-atz-*oba* at 273 and 298 K and afforded C_2H_4 and CO_2 uptakes that are in good agreement with the corresponding experimental measurements at low

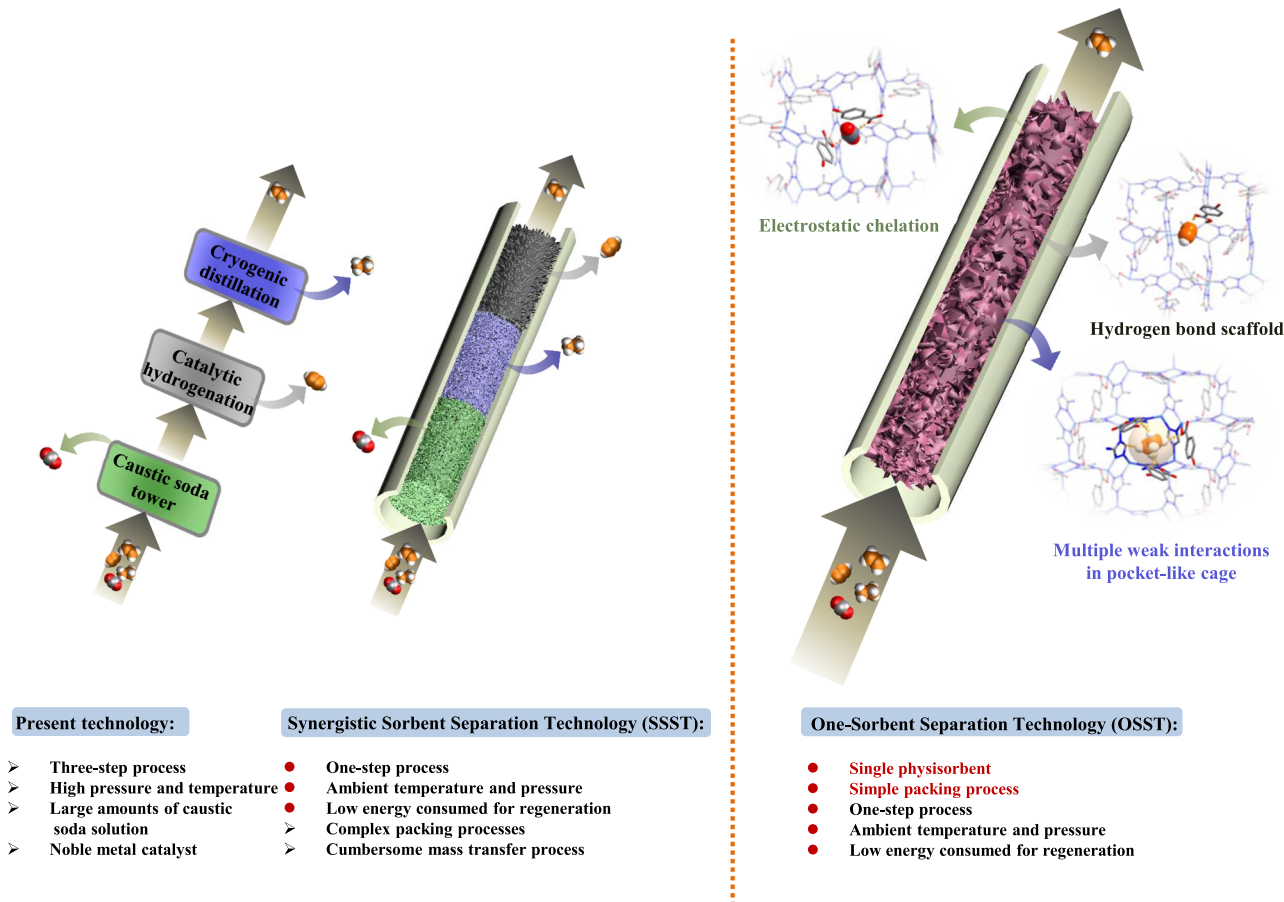


Fig. 1 Comparison of ethylene purification technologies. State-of-the-art separation technology is compared to synergistic sorbent separation technology (SSST) and “one-sorbent separation technology”, OSST.

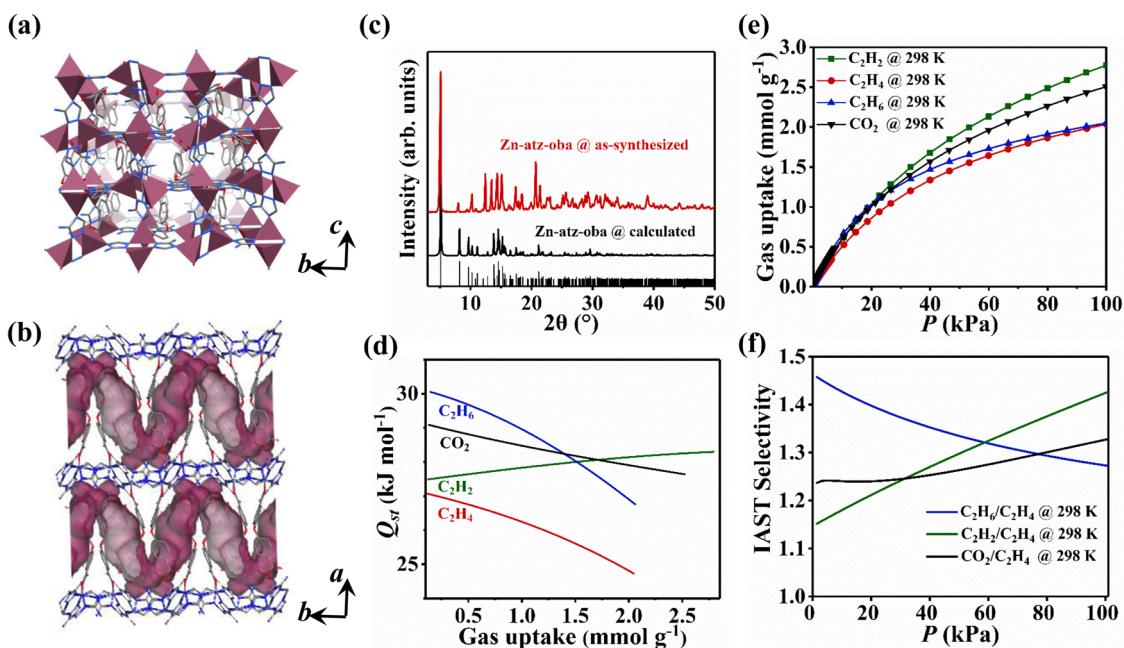


Fig. 2 Pore structure and gas sorption properties of Zn-atz-oba. Views of (a) the pore structure and (b) the Connolly surface of Zn-atz-oba when viewed along the *a*- and *c*-axis, respectively. H-atoms are omitted for clarity. (c) PXRD patterns confirm the bulk phase purity of Zn-atz-oba. (d) Adsorption enthalpy profiles (Q_{st}) for Zn-atz-oba. (e) Gas sorption isotherms of Zn-atz-oba at 298 K. (f) Binary 1:1 (v/v) IAST selectivity of Zn-atz-oba at 298 K. color codes for (a) and (b): carbon = gray; nitrogen = blue; oxygen = red; Zn polyhedra in (a) = tyrian purple; Connolly surface in (b) = purple.

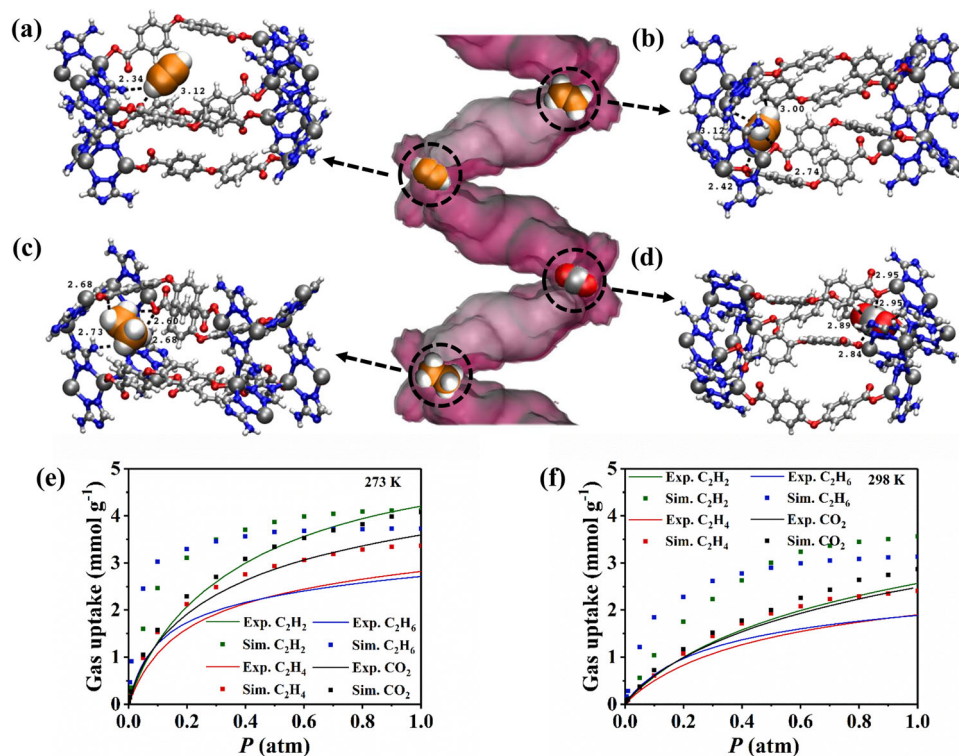


Fig. 3 Molecular modeling guided determination of primary adsorption sites and adsorption isotherms in Zn-atz-oba. The primary adsorption sites of (a) C₂H₂, (b) C₂H₄, (c) C₂H₆, and (d) CO₂ in Zn-atz-oba. Adsorbed gas molecules are presented in space-filling mode. color codes: C (Zn-atz-oba and CO₂): gray; C (C₂ gases): orange; H: white; O: red; N: blue; Zn: silver. Experimental (solid lines with circles) and simulated (squares) adsorption isotherms for C₂H₂ (green), C₂H₄ (red), C₂H₆ (blue), and CO₂ (black) at (e) 273 K and (f) 298 K and pressures up to 1 atm in Zn-atz-oba.

pressure (≤ 0.2 atm), but are slightly higher than experimental values at higher pressures (Fig. 3). Moreover, it can be observed that the simulated uptakes for C₂H₂ and C₂H₆ significantly overestimate their corresponding experimental values for most of the state points considered. Since polarization contributes to less than 10% of the total energy for simulations of all four gases in Zn-atz-oba (see Supplementary Fig. 21), the overestimation of the theoretical uptakes compared with experiment might be attributable to the partial charges (Supplementary Data 1) and/or the repulsion/dispersion parameters (Supplementary Data 2) that were used for the MOF atoms (for crystallographic distances between MOF atoms see Supplementary Data 3; further details of the modeling study are provided in Supplementary Note 3: Modeling Study). Future work could exploit multiple MOF force field parameters for the simulations and investigate their effect upon the reliability of gas uptakes in this material. Although the simulated uptakes in Zn-atz-oba are inconsistent with experimental data, the simulations still properly predicted that this material exhibits the lowest uptake for C₂H₄ within the considered pressure range at 273 and 298 K. In addition, according to the simulations, Zn-atz-oba was expected to display higher uptake for C₂H₆ within the low-pressure region (< 0.1 atm) compared to the other three gases. This is also consistent with the finding that this other MOF exhibited the highest initial Q_{st} value toward C₂H₆ according to both experiment and simulation (Fig. 2d and Supplementary Table 4).

Molecular simulations revealed that the most favorable binding site for all adsorbates lies within the confined region enclosed by four atz linkers and three oba linkers (Fig. 3). In this region, C₂H₂ interacts with the -NH₂ group of atz with N...H...C distances of 2.34 Å (Fig. 3a). C₂H₄, C₂H₆, and CO₂ exhibit different orientations than C₂H₂, which allow them to make multiple

contacts with the surrounding atoms of the framework. Most sorbent-sorbate interaction distances are longer for C₂H₄ versus C₂H₆ and CO₂, indicating weaker interactions between C₂H₄ and the pores of Zn-atz-oba (Fig. 3b-d). The GCMC-calculated initial Q_{st} values were determined and exhibit the following trend: C₂H₆ > CO₂ > C₂H₂ > C₂H₄ (see Supplementary Table 4). The greater Q_{st} value for C₂H₆ versus CO₂ in Zn-atz-oba is supported by shorter interactions between C₂H₆ and Zn-atz-oba, perhaps because of the larger molecular dimensions of C₂H₆ and repulsive interactions between the negatively charged O atoms of CO₂ and the surrounding electronegative N atoms of the atz linkers at the binding site. Further, the close N...H...C interactions exhibited by C₂H₂ are shorter than those of C₂H₄. Overall, the modeling studies support the experimental finding that C₂H₄ forms weaker interactions with Zn-atz-oba than the other three gases.

Breakthrough experiments of Zn-atz-oba. The gas separation performance was determined by dynamic column breakthrough experiments performed with Zn-atz-oba. In a typical breakthrough test at 298 K and ambient pressure, C₂H₄/C₂H₆, C₂H₂/C₂H₄/C₂H₆, and C₂H₂/C₂H₄/C₂H₆/CO₂ mixtures (equimolar mixtures, total gas pressure = 100 kPa) were passed through a packed column and the effluent streams were monitored by gas chromatography. In accordance with the pure gas sorption results and the molecular simulations derived understanding of the binding sites, the Zn-atz-oba fixed-bed column eluted C₂H₄ with ultra-high purity in a single step from all three gas mixtures. As shown in Fig. 4a-c, C₂H₄ breaks through first at ca. 236, 177, and 130 min, respectively, and the impurities (C₂H₆, C₂H₂, and CO₂) break through 14, 12, and 10 min later, respectively. Before breakthrough of C₂H₆, C₂H₄ of polymer grade purity (>99.95%) was collected at the outlet, revealing that Zn-atz-oba achieved

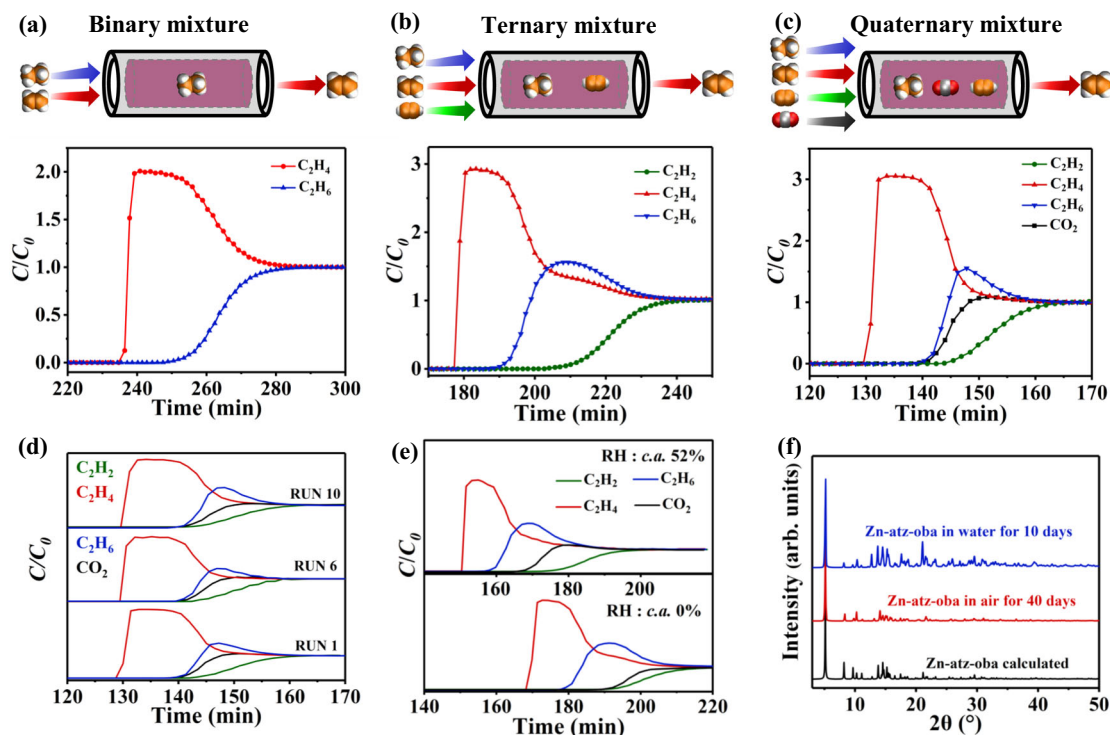


Fig. 4 Dynamic breakthrough experiments and stability tests. (a)–(c) Experimental breakthrough curves at 298 K for C_2H_4/C_2H_6 (1:1) (a), $C_2H_2/C_2H_4/C_2H_6$ (1:1:1) (b), and $C_2H_2/C_2H_4/C_2H_6/CO_2$ (1:1:1:1) (c) separations (equimolar mixtures; total gas pressure 100 kPa; total gas flow 1.4, 2.1 and $2.8\text{ cm}^3\text{ min}^{-1}$, respectively) based on Zn-atz-oba (6.3 g) packed column (C: Outlet gas concentration, C_0 : Inlet gas concentration). (d) Dynamic breakthrough data obtained with Zn-atz-oba fixed-bed in 1st, 5th, and 10th cycle when subjected to four-component $C_2H_2/C_2H_4/C_2H_6/CO_2$ (1:1:1:1) mixture. (e) Four-component (1:1:1:1) breakthrough experiment in the presence of water vapor at 288 K and 100 kPa based on Zn-atz-oba (7.0 g) packed column (total gas flow of $2.8\text{ cm}^3\text{ min}^{-1}$). (f) PXRD patterns of Zn-atz-oba after being subjected to air exposure and water immersion stability test conditions.

one-step purification of C_2H_4 by the coadsorption of C_2H_2 , C_2H_6 , and CO_2 from $C_2H_2/C_2H_4/C_2H_6/CO_2$ (>99.95% C_2H_4 productivity, 0.106 mmol g^{-1}). To explore the recycling performance of Zn-atz-oba, ten cycles of four-component breakthrough experiments were conducted. There was no loss of C_2H_4 retention time (Fig. 4d). In industrial C2 hydrocarbon gas streams, C_2H_2 only constitutes ~1% of the total flow⁵⁰. We also tested a $C_2H_2/C_2H_4/C_2H_6/CO_2$ (1/33/33/33) mixture under dynamic breakthrough using 7.4 g Zn-atz-oba packed in a fixed-bed. As shown in Fig. S25, polymer-grade ethylene was harvested from 1/33/33/33 gas mixture, followed by C_2H_6 , CO_2 , and C_2H_2 . As a typical contaminant in downstream feedstocks, water vapor is present in the industrially produced C2- CO_2 stream⁵¹, so breakthrough experiments in the presence of water vapor were conducted. As revealed by Fig. 4e, fractional pressure reduction of C_2H_2 , C_2H_4 , C_2H_6 , and CO_2 in the presence of water vapor reduced the adsorption capacity of Zn-atz-oba. This is reflected in a reduced C_2H_4 breakthrough time, from *c.a.* 170 min to *c.a.* 150 min. 4-component $C_2H_2/C_2H_4/C_2H_6/CO_2$ (1:1:1:1) breakthrough experiments in the presence of water vapor (relative humidity 52%) also resulted in a reduced retention time but a consistent gas outflow sequence. Nevertheless, C_2H_4 with effluent purity >99.95% was collected at the column outlet. We attribute the shorter retention time under 52% humidity to the presence of water vapor in the breakthrough pipeline and competing sorption of water with the other four gases. After ambient air exposure for 30 days or water immersion for 10 days, PXRD patterns (Fig. 4f) and N_2 isotherms at 77 K (including pore distribution, Supplementary Figs. 26 and 27) of regenerated Zn-atz-oba indicated that it is stable to both humid air and liquid water. Temperature-

programmed desorption of the fully adsorbed column was conducted after achieving full saturation and revealed that the Zn-atz-oba bed could be regenerated within 50 min at 333 K under He flow ($30\text{ cm}^3\text{ min}^{-1}$). Even under ambient conditions (298 K and 100 kPa), regeneration was achieved within 140 min under He flow of $20\text{ cm}^3\text{ min}^{-1}$ (Supplementary Fig. 23), confirming that there is indeed a relatively low energy footprint for Zn-atz-oba regeneration.

Discussion

If one compares the performances of previously reported physisorbents in the context of ethylene purification from binary mixtures^{15–20,22–30,32,46} (C_2H_2/C_2H_4 , C_2H_6/C_2H_4 , and C_2H_4/CO_2) and ternary mixtures^{35,36,39–41} ($C_2H_2/C_2H_4/C_2H_6$, $C_2H_2/C_2H_4/CO_2$, and $C_2H_6/C_2H_4/CO_2$), it is evident that Zn-atz-oba represents a benchmark in terms of its performance parameters (Fig. 5). Specifically, Zn-atz-oba coadsorbs three gases, C_2H_2 , C_2H_6 , and CO_2 , to produce polymer-grade (>99.95%) C_2H_4 in just one step. We attribute this performance to the unusual pore environment in Zn-atz-oba, which enables roughly equal affinity towards C_2H_2 , C_2H_6 , and CO_2 over C_2H_4 . Future studies will focus upon crystal engineering of second-generation variants to further improve the purification performances of other gas mixtures of industrial relevance.

Methods

General. All reagents were obtained from vendors and used as received without further purification. Powder X-ray diffraction (PXRD) data were collected with a Rigaku-Miniflex-600 diffractometer at a scanning rate of 5° min^{-1} using $Cu\ K_\alpha$ radiation. Thermogravimetric analysis (TGA) data were obtained using Mettler TG DSC 3+ Thermogravimetric Analyzer. In TGA measurements, the sample was

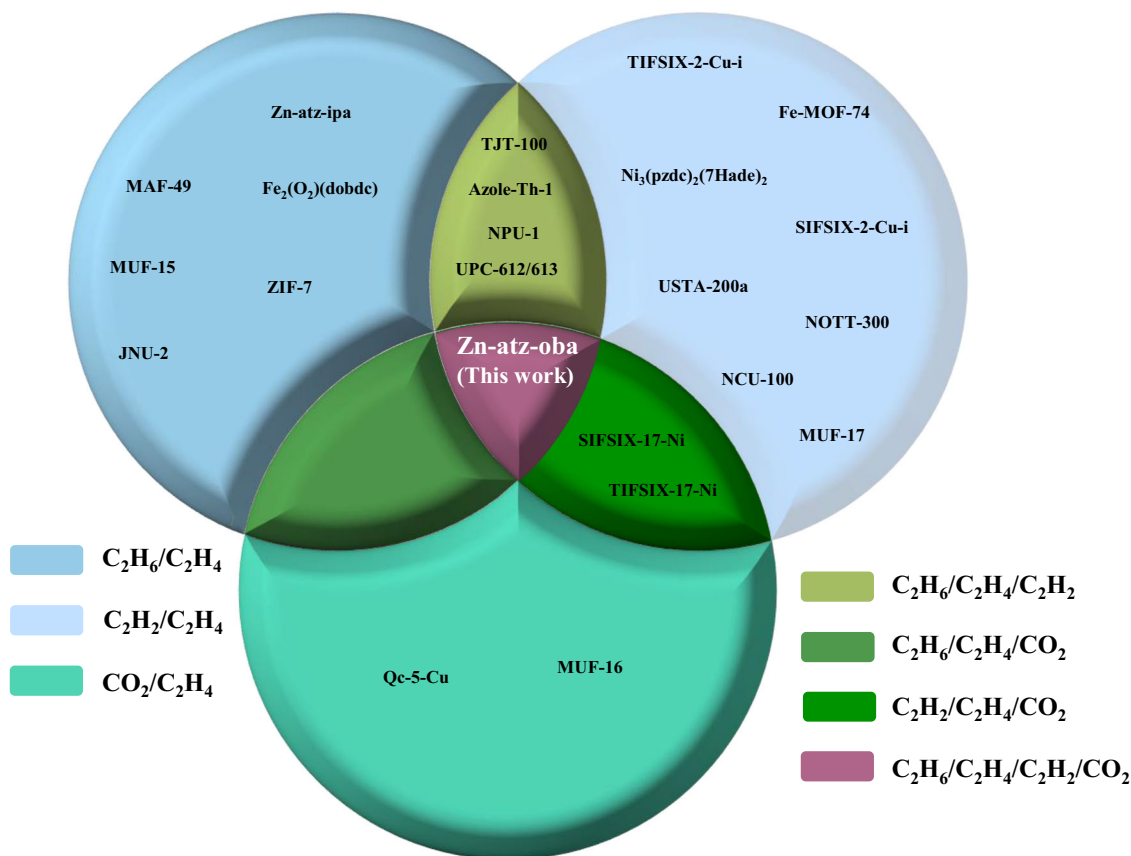


Fig. 5 Physisorbents studied for C_2H_4 purification. Comparison of physisorbents that can purify C_2H_4 from binary (sky blue)^{15–20, 22–30, 32, 46}, ternary (olive green)^{35, 36, 39–41} and quaternary mixtures (lilac, this work) under ambient conditions.

heated from 298 K to 1073 K under Ar atmosphere at a heating rate of 10 K min^{-1} . The morphology was examined using scanning electron microscopy (FESEM, Verios G4, FEI).

Synthesis of Zn-atz-oba. A mixture of $Zn(NO_3)_2 \cdot 6H_2O$ (10 mmol, 2.98 g), H_2oba (5 mmol, 1.29 g), Hatz (10 mmol, 0.84 g), DMF (40 mL), MeOH (40 mL), and H_2O (20 mL) was sealed in a 250 ml borosilicate bottle and sonicated for five minutes. The reaction mixture was then solvothermally treated at 403 K for 3 days before naturally cooling it to room temperature. The as-synthesized sample Zn-atz-oba was washed with fresh DMF, MeOH, and H_2O , and exchanged with MeOH three times daily for three days and then activated at 353 K in vacuum for 12 h.

Single-component gas sorption experiments. A Micromeritics 3Flex was used for recording all gas sorption isotherms, N_2 (77 K), C_2H_2 , C_2H_4 , C_2H_6 , and CO_2 (each, 273 and 298 K). For N_2 adsorption isotherms, the temperature was controlled at 77 K using a Dewar containing 4 L liquid N_2 . Precise control of 273 and 298 K temperatures was implemented by a dc-2006 from Ningbo Scientz Biotechnology, which contained a cyclic control system of ethylene glycol and water mixture ($v/v = 1:1$). Zn-atz-oba was degassed at 298 K under high vacuum for 4 h to regenerate in between consecutive isotherm measurements.

Dynamic gas breakthrough experiments. Breakthrough curves were recorded by an in-house custom-built rig (Supplementary Fig. 22). Equimolar C_2H_6/C_2H_4 (1:1), $C_2H_2/C_2H_4/C_2H_6$ (1:1:1) and $C_2H_2/C_2H_4/C_2H_6/CO_2$ (1:1:1:1) gas mixtures (total gas pressure and flow: 100 kPa and 1.4, 2.1, and $2.8\text{ cm}^3\text{ min}^{-1}$, respectively) were subjected through the Zn-atz-oba packed column (6.3 g) at 298 K, and the outlet gas concentrations and composition were monitored by a gas chromatography analyzer (Carrier gas: He, TCD-Thermal Conductivity Detector, detection limit 0.1 ppm). During gas breakthrough cycling tests, Zn-atz-oba packed in the column was regenerated under He flow of $30\text{ cm}^3\text{ min}^{-1}$ at 333 K for 2 h, after each breakthrough experiment.

Data availability

The sorption data; molecular simulations and breakthrough data generated in this study are provided in the Supplementary Information/Source Data file⁵².

Code availability

The codes used to analyse all the data generated in this study are provided in the Supplementary Information (Supplementary Note 1: Calculations, Supplementary Note 2: Adsorption enthalpy calculation and Supplementary Note 3: Modeling Study) and/or the Source Data file⁵².

Received: 19 April 2021; Accepted: 6 October 2021;

Published online: 11 November 2021

References

- Ethylene (ET): 2019 World Market Outlook and Forecast up to 2023. <https://www.researchandmarkets.com/> (retrieved Jan 2019).
- Sholl, D. S. & Lively, R. P. Seven chemical separations to change the world. *Nature* **532**, 435–437 (2016).
- Sadrameli, S. M. Thermal/catalytic cracking of hydrocarbons for the production of olefins: a state-of-the-art review I: thermal cracking review. *Fuel* **140**, 102–115 (2015).
- Safarik, D. J. & Eldridge, R. B. Olefin/paraffin separations by reactive absorption: a review. *Ind. Eng. Chem. Res.* **37**, 2571–2581 (1998).
- Ren, T., Patel, M. & Blok, K. Olefins from conventional and heavy feedstocks: energy use in steam cracking and alternative processes. *Energy* **31**, 425–451 (2006).
- P. A. Angelini, T et al. Materials for Separation Technologies: Energy and Emission Reduction Opportunities. Oak Ridge, TN (United States): Oak Ridge National Lab. (ORNL); 2005.
- Wang, H., Liu, Y. & Li, J. Hydrocarbon separation: designer metal-organic frameworks for size-exclusion-based hydrocarbon separations: progress and challenges. *Adv. Mater.* **32**, 2002603 (2020).
- Li, J., Kuppler, R. J. & Zhou, H. Selective gas adsorption and separation in metal-organic frameworks. *Chem. Soc. Rev.* **38**, 1477–1504 (2009).

9. Perry, J. J., Perman, J. A. & Zaworotko, M. J. Design and synthesis of metal-organic frameworks using metal-organic polyhedra as supermolecular building blocks. *Chem. Soc. Rev.* **38**, 1400–1417 (2009).
10. MacGillivray L.-R. *Metal-Organic Frameworks: Design and Application* (ed. MacGillivray, L.-R.) (Wiley, Hoboken, NJ, 2010).
11. Furukawa, H., Cordova, K. E., O’Keeffe, M. & Yaghi, O. M. The chemistry and applications of metal-organic frameworks. *Science* **341**, 1230444 (2013).
12. Kitagawa, S., Kitaura, R. & Noro, S. Functional porous coordination polymers. *Angew. Chem. Int. Ed.* **43**, 2334–2375 (2004).
13. Mukherjee, S., Sensharma, D., Chen, K. & Zaworotko, M. J. Crystal engineering of porous coordination networks to enable separation of C₂ hydrocarbons. *Chem. Commun.* **56**, 10419–10441 (2020).
14. Yang, H. et al. Pore-Space-Partition-Enabled exceptional ethane uptake and ethane-selective ethane-ethylene separation. *J. Am. Chem. Soc.* **142**, 2222–2227 (2020).
15. Liao, P., Zhang, W., Zhang, J. & Chen, X. Efficient purification of ethene by an ethane-trapping metal-organic framework. *Nat. Commun.* **6**, 8697 (2015).
16. Qazvini, O. T., Babarao, R., Shi, Z., Zhang, Y. & Telfer, S. G. A robust ethane-trapping metal-organic framework with a high capacity for ethylene purification. *J. Am. Chem. Soc.* **141**, 5014–5020 (2019).
17. Sun, F. et al. Microporous metal-organic framework with a completely reversed adsorption relationship for C₂ hydrocarbons at room temperature. *ACS Appl. Mater. Interfaces* **12**, 6105–6111 (2020).
18. Li, L. et al. Ethane/ethylene separation in a metal-organic framework with iron-peroxo sites. *Science* **362**, 443–446 (2018).
19. Zeng, H. et al. Cage-Interconnected metal-organic framework with tailored apertures for efficient C₂H₆/C₂H₄ separation under humid conditions. *J. Am. Chem. Soc.* **141**, 20390–20396 (2019).
20. Gücüyener, C., van den Bergh, J., Gascon, J. & Kapteijn, F. Ethane/Ethene separation turned on its head: Selective ethane adsorption on the metal-organic framework ZIF-7 through a gate-opening mechanism. *J. Am. Chem. Soc.* **132**, 17704–17706 (2010).
21. Lysova, A. A. et al. A series of mesoporous metal-organic frameworks with tunable window sizes and exceptionally high ethane over ethylene adsorption selectivity. *Angew. Chem. Int. Ed.* **59**, 20561–20567 (2020).
22. Bloch, E. D. et al. Hydrocarbon separations in a metal-organic framework with open iron (II) coordination sites. *Science* **335**, 1606–1610 (2012).
23. Zhang, Z. et al. Efficient trapping of trace acetylene from ethylene in an ultramicroporous metal-organic framework: synergistic effect of high-density open metal and electronegative sites. *Angew. Chem. Int. Ed.* **59**, 18927–18932 (2020).
24. Cui, X. et al. Pore chemistry and size control in hybrid porous materials for acetylene capture from ethylene. *Science* **353**, 141–144 (2016).
25. Li, B. et al. An ideal molecular sieve for acetylene removal from ethylene with record selectivity and productivity. *Adv. Mater.* **29**, 1704210 (2017).
26. Chen, K. et al. Benchmark C₂H₂/CO₂ and CO₂/C₂H₂ separation by two closely related hybrid ultramicroporous materials. *Chem* **1**, 753–765 (2016).
27. Yang, S. et al. Supramolecular binding and separation of hydrocarbons within a functionalized porous metal-organic framework. *Nat. Chem.* **7**, 121–129 (2015).
28. Wang, J. et al. Optimizing pore space for flexible-robust metal-organic framework to boost trace acetylene removal. *J. Am. Chem. Soc.* **142**, 9744–9751 (2020).
29. Qazvini, O. T., Babarao, R. & Telfer, S. G. Multipurpose metal-organic framework for the adsorption of acetylene: ethylene purification and carbon dioxide removal. *Chem. Mater.* **31**, 4919–4926 (2019).
30. He, T., Xiao, Y., Zhao, Q., Zhou, M. & He, G. Ultramicroporous metal-organic framework Qc-5-Cu for highly selective adsorption of CO₂ from C₂H₄ stream. *Ind. Eng. Chem. Res.* **59**, 3153–3161 (2020).
31. Horike, S. et al. Dense coordination network capable of selective CO₂ capture from C₁ and C₂ hydrocarbons. *J. Am. Chem. Soc.* **134**, 9852–9855 (2012).
32. Qazvini, O. T., Babarao, R. & Telfer, S. G. Selective capture of carbon dioxide from hydrocarbons using a metal-organic framework. *Nat. Commun.* **12**, 197 (2021).
33. Mukherjee, S. & Zaworotko, M. J. Crystal engineering of hybrid coordination networks: from form to function. *Trends Chem.* **2**, 506–518 (2020).
34. Liu, S. et al. Efficient separation of acetylene and carbon dioxide in a decorated zeolite. *Angew. Chem. Int. Ed.* **60**, 6526–6532 (2021).
35. Hao, H. G. et al. Simultaneous trapping of C₂H₂ and C₂H₆ from a ternary mixture of C₂H₂/C₂H₄/C₂H₆ in a robust metal-organic framework for the purification of C₂H₄. *Angew. Chem. Int. Ed.* **57**, 16067–16071 (2018).
36. Xu, Z. et al. A robust Th-azole framework for highly efficient purification of C₂H₄ from a C₂H₄/C₂H₂/C₂H₆ mixture. *Nat. Commun.* **11**, 3163 (2020).
37. Dong, Q. et al. Tuning gate-opening of a flexible metal-organic framework for ternary gas sieving separation. *Angew. Chem. Int. Ed.* **59**, 22756–22762 (2020).
38. Yang, S. et al. Efficient purification of ethylene from C₂ hydrocarbons with an C₂H₆/C₂H₂-selective metal-organic framework. *ACS Appl. Mater. Interfaces* **13**, 962–969 (2021).
39. Zhu, B. et al. Pore engineering for one-step ethylene purification from a three-component hydrocarbon mixture. *J. Am. Chem. Soc.* **143**, 1485–1492 (2021).
40. Mukherjee, S. et al. Amino-Functionalised hybrid ultramicroporous materials that enable single-step ethylene purification from a ternary mixture. *Angew. Chem. Int. Ed.* **60**, 10902–10909 (2021).
41. Wang, Y. et al. One-step ethylene purification from an acetylene/ethylene/ethane ternary mixture by cyclopentadiene cobalt-functionalized metal-organic frameworks. *Angew. Chem. Int. Ed.* **60**, 11350–11358 (2021).
42. O’Hearn, D. J., Bajpai, A. & Zaworotko, M. J. The “Chemistree” of porous coordination networks: taxonomic classification of porous solids to guide crystal engineering studies. *Small* **2006351** (2021).
43. Nugent, P. et al. Porous materials with optimal adsorption thermodynamics and kinetics for CO₂ separation. *Nature* **495**, 80–84 (2013).
44. Lin, R. et al. Molecular sieving of ethylene from ethane using a rigid metal-organic framework. *Nat. Mater.* **17**, 1128–1133 (2018).
45. Liao, P., Huang, N., Zhang, W., Zhang, J. & Chen, X. Controlling guest conformation for efficient purification of butadiene. *Science* **356**, 1193–1196 (2017).
46. Chen, K. et al. Synergistic sorbent separation for one-step ethylene purification from a four-component mixture. *Science* **366**, 241–246 (2019).
47. Chen, K. et al. New Zn-aminotriazolate-dicarboxylate frameworks: synthesis, structures, and adsorption properties. *Cryst. Growth Des.* **13**, 2118–2123 (2013).
48. Spek, A. L. Structure validation in chemical crystallography. *Acta Cryst.* **D65**, 148–155 (2009).
49. Myers, A. L. & Prausnitz, J. M. Thermodynamics of mixed-gas adsorption. *AIChE J.* **11**, 121–127 (1965).
50. Bao, Z. et al. Potential of microporous metal-organic frameworks for separation of hydrocarbon mixtures. *Energy Environ. Sci.* **9**, 3612–3641 (2016).
51. Yancheshmeh, M. S. S. et al. Modeling of ethane pyrolysis process: a study on effects of steam and carbon dioxide on ethylene and hydrogen productions. *Chem. Eng. J.* **215–216**, 550–560 (2013).
52. Jian-Wei, C. (2021): Zn-atz-oba gas sorption data (Exp. and Sim.) is provided as a Figshare dataset: <https://doi.org/10.6084/m9.figshare.16571151.v1>.

Acknowledgements

K.J.C. acknowledges the National Natural Science Foundation of China (grant number 22071195, 21805227) and Fundamental Research Funds for the Central Universities (grant number 3102017j01001). T.W. acknowledges the National Natural Science Foundation of China (grant number 21905229). M.J.Z. acknowledges the Science Foundation Ireland (awards 13/RP/B2549, 16/IA/4624) and the European Research Council (award ADG 885695). S.M. acknowledges the Alexander von Humboldt Foundation for the award of a postdoctoral research fellowship. We would like to thank the Analytical & Testing Center of Northwestern Polytechnical University and cceshi (www.cceshi.com) for SEM and TGA testing, respectively. T.P., K.A.F., and B.S. acknowledge the National Science Foundation (Award No. DMR-1607989), including support from the Major Research Instrumentation Program (Award No. CHE-1531590). Computational resources were made available by a XSEDE Grant (No. TG-DMR090028) and by Research Computing at the University of South Florida.

Author contributions

K.J.C. and M.J.Z. designed the project. J.W.C. and H.J.T. synthesized the compounds. J.W.C. collected and analyzed all adsorption data. T.Z. and T.W. collected and analyzed the power X-ray diffraction. T.P., K.A.F., and B.S. performed the classical molecular simulations. J.W.C., S.M., and X.J. collected the experimental breakthrough data. S.M. and Y.W. contributed to formal analysis and data curation. J.W.C., S.M., and K.J.C. wrote the paper, and all authors contributed to revise the manuscript.

Competing interests

The authors declare no competing interests.

Additional information

Supplementary information The online version contains supplementary material available at <https://doi.org/10.1038/s41467-021-26473-8>.

Correspondence and requests for materials should be addressed to Michael J. Zaworotko or Kai-Jie Chen.

Peer review information *Nature Communications* thanks the anonymous reviewer(s) for their contribution to the peer review of this work.

Reprints and permission information is available at <http://www.nature.com/reprints>

Publisher’s note Springer Nature remains neutral with regard to jurisdictional claims in published maps and institutional affiliations.



Open Access This article is licensed under a Creative Commons Attribution 4.0 International License, which permits use, sharing, adaptation, distribution and reproduction in any medium or format, as long as you give appropriate credit to the original author(s) and the source, provide a link to the Creative Commons license, and indicate if changes were made. The images or other third party material in this article are included in the article's Creative Commons license, unless indicated otherwise in a credit line to the material. If material is not included in the article's Creative Commons license and your intended use is not permitted by statutory regulation or exceeds the permitted use, you will need to obtain permission directly from the copyright holder. To view a copy of this license, visit <http://creativecommons.org/licenses/by/4.0/>.

© The Author(s) 2021